Available online at www.sciencedirect.com
ScienceDirect
Nuclear Instruments and Methods in Physics Research A 580 (2007) 1310–1326
NUCLEAR INSTRUMENTS & METHODS IN PHYSICS RESEARCH Section A
www.elsevier.com/locate/nima

A detector for filtering γ-ray spectra from weak fusion–evaporation reactions out of strong background and for Doppler correction: The recoil filter detector, RFD

W. Męczyński[a,*], P. Bednarczyk[a,b], J. Grębosz[a], J. Heese[c], M. Janicki[a], K.H. Maier[a], J.C. Merdinger[d], K. Spohr[e], M. Zięblíński[a], J. Styczeń[a]

[a]*The Henryk Niedwodniczański Institute of Nuclear Physics, Polish Academy of Sciences, ul. Radzikowskiego 152, 31-342 Kraków, Poland*
[b]*Gesellschaft für Schwerionenforschung mbH, Planckstr. 1, D-64291 Darmstadt, Germany*
[c]*ACCEL Instruments GmbH, Friedrich-Ebert-Str. 1, 51429 Bergisch Gladbach, Germany*
[d]*Institut de Recherches Subatomiques, 23, Rue du Loess, 67037 Strasbourg, France*
[e]*University of Paisley, Paisley PA1 2BE, Scotland, UK*

Received 10 May 2007; received in revised form 19 July 2007; accepted 20 July 2007
Available online 1 August 2007

Abstract

A detector has been designed and built to assist in-beam γ-ray spectroscopy with fusion–evaporation reactions. It measures with high efficiency the evaporation residues that recoil out of a thin target into the angular interval from 1.8° to 9.0° at an adjustable distance of 1000–1350 mm from a target, in coincidence with γ-rays detected in a Ge-detector array. This permits filtering of such γ-rays out of a much stronger background of other reaction products and scattered beam. Evaporation residues are identified by their time-of-flight and the pulse height using a pulsed beam. The velocity vector of the γ-emitting recoil is also measured in the event-by-event mode, facilitating to correct the registered γ-ray energy for the Doppler shift, with the resulting significant improvement of the energy resolution. The heavy-ion detection scheme uses emission of secondary electrons caused by the recoiling ions when hitting a thin foil. These electrons are then electrostatically accelerated and focused onto a small scintillator that measures the summed electron energy, which is proportional to the number of electrons. The detector is able to operate at high frequency of the order of 1 MHz and detect very heavy nuclei with as low kinetic energy as 5 MeV. The paper describes the properties of the detector and gives examples of measurements with the OSIRIS, GAREL+ and EUROBALL IV γ-ray spectrometers. The usefulness of the technique for spectroscopic investigations of nuclei with a continuous beam is also discussed.

PACS: 29.30.−h; 29.30.Kv; 29.40.Gx

Keywords: In-beam γ-ray spectroscopy; Evaporation residue detection; Doppler shift correction

1. Introduction

In-beam γ-ray spectroscopy with fusion–evaporation reactions using light and heavy ions is one of the major tools in nuclear structure research. At bombarding energies not too far above the Coulomb barrier, fusion–evaporation reactions are usually dominant with a cross-section of about 0.1–1 b. Often also a single nucleus is populated preferentially, and the γ-ray spectrum is then rather simple and easily interpreted. In these cases it is sufficient to measure only γ-spectra, usually multiple γ–γ coincidences. This changes, however, if one wants to study heavy nuclei, roughly beyond Pb; then the compound nucleus mostly undergoes fission, while particle evaporation leading to the nuclei of interest becomes weak. There are also regimes in which deep-inelastic reactions or Coulomb excitation dominate. In a situation like this, a positive identification and selection of the γ-rays from the rare wanted fusion–evaporation events is essential. Another frequent

*Corresponding author. Tel.: +48 12 662 8297; fax: +48 12 662 8423.
E-mail address: Witold.Meczynski@ifj.edu.pl (W. Męczyński).

0168-9002/$ - see front matter © 2007 Elsevier B.V. All rights reserved.
doi:10.1016/j.nima.2007.07.132

problem appears in thin target experiments, in which the γ-rays are emitted from the nuclei in flight and are therefore Doppler shifted. This is often the dominant contribution to the γ-ray energy resolution in light nuclei and might be as bad as to prevent a meaningful measurement. If, however, the velocity vector of the emitting nucleus is measured, the Doppler shift can be calculated and corrected precisely, overcoming this difficulty.

Therefore, a high-efficiency detector for evaporation residues, the Recoil Filter Detector (RFD), has been designed and built. Emission of secondary electrons induced by recoiling ions hitting a thin foil is used in the detection scheme. The emitted electrons are then accelerated and focused by electrostatic lenses onto a thin plastic scintillator providing a signal proportional to the number of the electrons. RFD distinguishes evaporation residues from other reaction products by their time-of-flight (ToF) and the pulse height, while it does not identify the element or nuclear mass. It measures also the velocity vector of the γ-ray emitting nucleus. Therefore, the Doppler shift of the γ-rays can be corrected individually for each event with the resulting significant improvement in resolution. Limiting the goals to these two points, namely filtering γ-rays from evaporation residues and measuring the velocity vector of the emitting nucleus, nonetheless, makes RFD a highly efficient tool for γ-ray spectroscopy investigations.

Mainly two other types of instruments have been used in spectroscopic studies with similar goals. The recoil mass spectrometers, such as the Fragment Mass Analyzer (FMA) [1] and the Recoil Mass Separator (RMS) [2], of dimensions of about 10 m, use big magnets and high electric fields to separate evaporation residues from the beam and to determine their masses precisely. However, their angular acceptance is small, resulting in low detection efficiency. Mass separators with gas filled magnets, like the Recoil Ion Transport Unit (RITU) [3], are used to detect evaporation residues with much higher detection efficiency, but without mass identification. Although the magnet has to be close to the target obstructing the space for forward detectors of the γ-ray detector array, the possibility of recoil-decay tagging makes this device best suited for investigation of exotic nuclei produced with extremely low cross-sections. However, this type of spectrometers is not able to provide information about ion tracks through active optic elements and, therefore, the Doppler correction in coincident γ-ray spectrum is not possible.

The use of the entrance and focal plane detectors, providing the position, time and energy signals in the Variable Mode High Acceptance Spectrometer (VAMOS) [4] at GANIL and in the PRISMA spectrometer [5] at LNL, allows for reconstruction of the ion trajectories. Time-of-flight information together with ion tracking is used to determine the velocity vector of ions, allowing for Doppler correction for coincident γ-rays on an event-by-event basis. However, VAMOS is primarily intended to be used to study proton-reach and transuranic nuclei with the SPIRAL low-intensity secondary beams. The PRISMA spectrometer is dedicated to investigate nuclei produced in multinucleon transfer, deep inelastic and fusion–fission reactions with stable and exotic beams.

Recently, another high-efficiency detector of evaporation residues, named HERCULES [6], has been built and used in in-beam experiments with the GAMMASPHERE γ-ray spectrometer. The HERCULES detector follows in much the principles of RFD in separation of evaporation residues by time-of-flight technique and pulse-height analysis. The main difference to RFD is that the evaporation residues are detected directly by thin fast plastic scintillators. HERCULES is anticipated to be used in γ-ray spectroscopic investigations of trans-lead nuclei.

RFD is intended to be used only in conjunction with γ-ray spectrometers. The first version has been built for the OSIRIS spectrometer [7] at HMI in Berlin. The second one has been designed for the GAREL + project [8] and then for the EUROBALL phase IV Ge-detector array at IReS in Strasbourg [9]. Section 2 presents the conceptual and overall design of RFD, and in Section 3 its main parts are treated in more detail. Section 4 gives the measured properties and performance of RFD in actual experiments with pulsed and continuous beams. They are followed by a summary, comparison with other detectors and an outlook on possible applications, in Section 5.

2. Conceptual design

The heavy-ion beam hits a thin target and causes nuclear reactions. The target is surrounded by a γ-ray detector array that measures the γ-radiation emitted from the reaction products. The nuclei that are produced in a fusion–evaporation reaction—the evaporation residues—have on the average the momentum of the beam particles. They, therefore, fly out of the thin target into a relatively narrow cone. The recoil due to evaporated particles and multiple scattering of the nuclei in the target determine the width of that cone. RFD detects the evaporation residues and thus provides signals that they have occurred. The principle difficulty of this scheme is that also the beam passing through the target with a particle flux that is many orders of magnitude more intense than that of evaporation residues would completely block any usual detector placed close to the beam axis, as a typical beam current for these experiments is 10^{10} particles/s, while the goal is to measure events down to a production rate of 10 evaporation residues/s. Thus, the angular range of scattered beam and evaporation residues overlap. The beam is however concentrated into a much narrower cone—typically 1–2°, depending on the target thickness—than the evaporation residues. RFD is therefore made sensitive only outward of a minimal angle of about 2°. The straggling in the target and consequently the target thickness is an essential parameter for partly separating evaporation residues and beam particles.

Considerations of the multiple scattering of the beam and of evaporation residues in the target and the resulting

angular and energy distributions show that the flux of beam particles can be reduced in this way by approximately a factor of 1000, while only about half of the wanted nuclei are lost.

The detector is segmented into individual detection elements closely packed in inner and outer concentric rings around the beam line. This granularity reduces the high rate of scattered beam particles in elements and gives the angle of emission of the detected nucleus for the Doppler correction. Nevertheless, the individual elements have still to tolerate of 10^6 beam particles/s and detect a few recoiling nuclei per second. Therefore, the detector has to be as fast as possible. Also, a detection scheme that gives a large signal for the slow heavy nuclei of interest and small signal for the scattered beam is clearly advantageous. This requirement is met, as the detector signal corresponds to the specific energy loss dE/dx rather than to the energy E of the particle. Because very slow heavy nuclei are to be measured with RFD, e.g. Th nuclei at 6 MeV, any gas detector like parallel plate avalanche counters [10] with a thin enough entrance foil would be prohibitively difficult.

As already stated, the secondary electron emission from a thin foil induced by recoiling ions [11] has been chosen as the "primary detection mechanism". The mechanism of this type, based on an isochronous transport of secondary electrons, was used successfully to suppress intense background from fission in γ-ray spectroscopy investigation of the ^{222}Th nucleus already in 1983 [12]. The total secondary electron yield γ_T from a foil is defined as the average number of secondary electrons emitted from the foil surfaces per incoming projectile. Rothard et al. [11] clearly demonstrated an overall proportionality between the secondary electron yield γ_T and the electronic energy loss dE/dx of the projectiles: $\gamma_T = \Lambda\, dE/dx$, with $\Lambda = 7$ (μg/cm^2)/keV in a wide range of projectile velocities and projectile nuclear charges. In order to produce the detector signal corresponding to the energy loss dE/dx, the number n_e of secondary electrons per incident ion has to be counted. This is accomplished by accelerating the simultaneously emitted electrons (of the order of 100) of low energy (of the order of 10 eV) with a voltage U (typically -20 kV) and focusing onto a thin plastic scintillator mounted on a photomultiplier (PM). The scintillator gives a signal corresponding to the absorbed energy ($n_e U = 2$ MeV) of the whole electron bunch and—in consequence—to the energy loss dE/dx of the ion in the foil. The focusing of electrons allows in addition to use smaller scintillators and PMs.

Evaporation residues differ significantly from other reaction products and beam particles in the velocity and therefore in their time-of-flights on a distance of the order of 1 m. RFD is designed for such a flight path and for a pulsed beam with a repetition time of several hundreds of nanoseconds. Individual RFD detection elements, particularly the inner ones, are hit by 1 beam particle per beam pulse in average. The decay time of the scintillation and the signal transit time of the PM should be short enough that after less than 50 ns the next particle, in particular the wanted evaporation residue, can be measured. The pulsed beam allows using a fast linear gate for the signals from the PM. The linear gate triggered by a synchronized signal from the pulsing system of the accelerator acts as a slit in time that discards the beam and lets the wanted particles pass. In this way, the following electronics are not overloaded by the high counting rate from the scattered beam.

The following RFD electronics require a coincidence with the γ-ray detector. If a valid γ-event coincides with the signal from RFD, the digitized pulse height and time-of-flight of the ion are stored together with the γ-ray data. Selecting events with the appropriate time-of-flight and the pulse height when sorting the data gives clean γ-ray spectra from very rare evaporation residues. The measured time-of-flight and the position of the RFD element fired determine the velocity vector of every nucleus that emitted the γ-rays. Consequently, the Doppler shift is measured precisely in the event-by-event mode and can be corrected with often a big gain in energy resolution.

3. Detection scheme and detector design

3.1. Energy and angular distribution of evaporation residues and scattered beam

The compound nucleus formed by fusion of a beam particle and a target nucleus has the momentum of the beam particle. Therefore, the compound nuclei show the same spread in angle as the beam. In the following it is assumed that in praxis we are using a well-defined parallel beam without a halo of particles at rather large angle and—consequently—the spread of the compound nuclei induced by the angular spread of the beam is negligible. Beam particles, that do not undergo a nuclear reaction, change their direction and energy when passing the target due to the multiple Rutherford scattering and interactions with the target electrons.

The recoil caused by particle evaporation from the compound nucleus broadens the momentum distribution of the evaporation residues. The angular and energy distributions of the evaporated particles are known well enough for our purpose. We take the angular distribution for neutrons as isotropic. For protons and α-particles, the differential cross-section is taken as $d\sigma/d\Omega = c/\sin\Theta + k$ for $\Theta > 10^\circ$ and $\Theta < 170^\circ$, while it is constant with the value at 10° for $\Theta < 10^\circ$and $\Theta > 170^\circ$. Both parameters c and k are positive and $d\sigma/d\Omega$ is about a factor of 3 smaller at 90° than at 0°, reflecting measured data [13]. A Monte Carlo code TRIMTRANS [14] was written, which includes the steps just mentioned and it calculates the resulting distributions of the beam particles and evaporation residues in energy and angle.

Gamma-ray spectroscopy of ^{199}At produced in the ^{175}Lu(^{28}Si,4n)^{199}At reaction at 141 MeV with the cross-section of 100 μb [8] is taken as an example of the

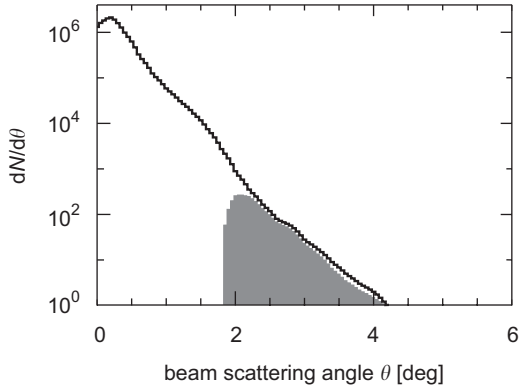

Fig. 1. Calculated angular distribution of 141 MeV ^{28}Si beam ions after passing a 0.7 mg/cm^2 thick ^{175}Lu target. 20 million events have been calculated and the number of ions per angular interval of 0.05° is plotted as a function of a beam-scattering angle. The shaded area presents the part of the distribution accepted by RFD as used with the GAREL + setup at a distance of 1330 mm from the target. Only 1.7% of the total number of the elastic scattered beam ions hit the sensitive area of RFD in this case.

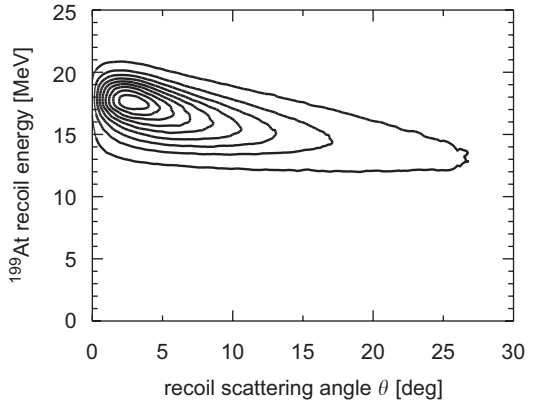

Fig. 2. Calculated distribution of ^{199}At recoils over their kinetic energy and scattering angle. The ^{199}At nuclei were produced by the ^{175}Lu (^{28}Si,4n)^{199}At reaction at 141 MeV in a 0.7 mg/cm^2 thick, metallic lutetium target. 4 million events have been calculated and the contour lines give number of recoils per angular and energy intervals of 0.2° and 126.5 keV in steps of 300 recoils with 2700 recoils in the peak of the distribution.

spectroscopy investigation of heavy nuclei. Fig. 1 shows the angular distribution of the ^{28}Si beam particles due to multiple scattering in the 0.7 mg/cm^2 ^{175}Lu target. At the GAREL + geometry (Section 4.1.1), only 1.7% of the total number of scattered beam particles—marked by the shaded area in Fig. 1—were accepted by the RFD detection elements, still giving an extremely high counting rate of the order of 10 MHz per element for a typical beam current of 10^{10} particles/s.

Two-dimensional distribution of the ^{199}At evaporation residues over kinetic energy and the scattering angle is calculated as follows. The reaction with the instantaneous process of particle evaporation can happen anywhere in the target and the final nucleus will then scatter on the remaining path through the target. Therefore the target is divided into 20 slices, in which the reaction might produce the At nuclei. At each of the target layers, the cross-section for the production of ^{199}At is calculated for the exact beam energy present at the entry to the layer. This assures that any variation with regard to the formation of ^{199}At is accounted for in the simulation program. The subdivision into a total of 20 different layers guarantees a high enough accuracy to avoid any computational artifacts that may arise from the introduced partitioning of layers. Because neutrons are emitted with little kinetic energy, the distribution due to their recoil is narrow in angle and energy. The energy loss and angular straggling in the remaining part of the target dominate the final distribution of the ^{199}At recoils. Straggling in the target is essential also in pulling beam and product nuclei apart and therefore the target thickness is an important experimental parameter. The resulting two-dimensional distribution of ^{199}At recoils is shown in Fig. 2 and its projection on the angle axis is presented in Fig. 3. The latter figure indicates also a high RFD acceptance of 27% of total number of emitted ^{199}At recoils at the GAREL + geometry. A comparison of the

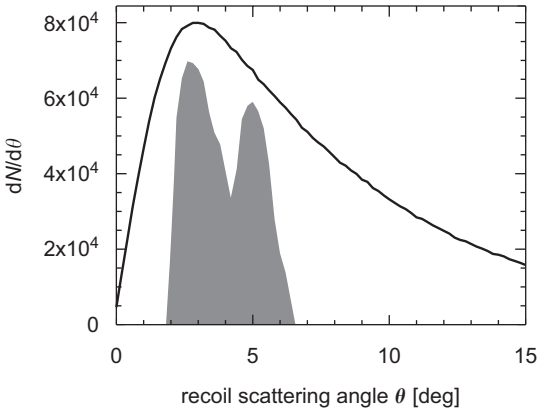

Fig. 3. Projection of the calculated distribution of the ^{199}At recoils of Fig. 2 on the scattering angle axis. The dark area shows the part of the angular distribution that RFD accepts at a distance of 1330 mm from a target at the GAREL + setup. In all, 27% of the total number of ^{199}At recoils emitted from the target can be detected by the recoil detector.

calculated RFD efficiency with the measured value for selected reaction is presented in Section 4.1.1.

The situation differs for light nuclei, particularly when protons and α-particles with much higher kinetic energies are emitted. The recoil due to emitted particles then governs the momentum distribution of the nuclei, while straggling of evaporation residues is less important. The ^{30}Si(^{18}O,p2n)^{45}Sc reaction with 68 MeV beam energy and a 0.8 mg/cm^2 metallic target is taken as example. The calculated distribution of ^{45}Sc recoils behind the target is shown in Fig. 4. The distribution is very wide both in scattering angle and kinetic energy. It has a maximum at about 4.5° and matches very well the angular acceptance of RFD placed at a distance of 1350 mm from the target (see Section 3.2). This good angular matching resulted in a high evaporation residue detection efficiency of 40% in spectroscopy measurements of $f_{7/2}$ nuclei with the EUROBALL IV array (Section 4.1.3).

3.2. Layout of the detector

A vertical cut through RFD used with the EUROBALL IV array on line of the VIVITRON accelerator at IReS in Strasbourg is given in Fig. 5. The forward half of the target chamber is seen at the left. The conical chamber connecting the target chamber with the detector tank can be varied in length to adjust a distance of the RFD electron-emitting foil array to the target from 1000 to 1350 mm (shown in the figure). It allows matching the flight path of recoils to the recoil velocity and the RFD acceptance angle to the angular distribution of evaporation residues. RFD consists of 18 cylindrical detection elements mounted in the inner ring of 6 and the outer ring of 12 elements around the beam axis. Four of them are seen in the detector tank to the right. The individual detection element is composed of the electron emitting foil under negative electrostatic potential, a set of electrodes accelerating and focusing the secondary electrons rejected from the foil by recoils, and a scintillation counter with a plastic scintillator mounted on a photomultipler tube (see Sections 3.3, 3.4 and 3.5 for details). The innermost central element is left out, and the bulk of the beam can pass through to a remote Faraday cup. The elements are tilted away from the axis, to protect scintillators against direct hits by beam particles scattered in the target. At the distance of 1350 mm, the half-opening angle of the individual detection element is about 1° and its solid angle is about 1 msr. At this distance, the array of 18 detection elements covers the angular interval from 1.8° to 6.7°. However, gaps between cylindrical elements cannot be avoided. The little covered area between the inner and the outer rings of elements is evident in the dip of the RFD sensitivity in Fig. 3. Therefore, the total solid angle of RFD

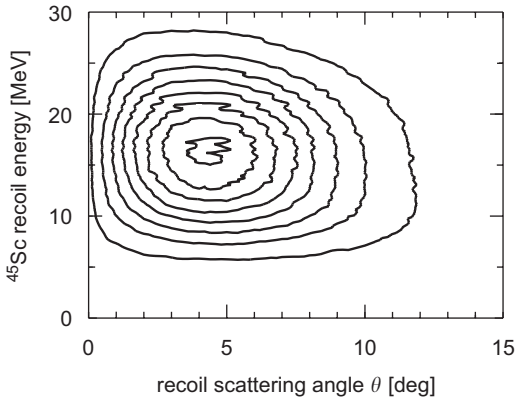

Fig. 4. Calculated distribution of ^{45}Sc nuclei from the ^{30}Si(^{18}O,p2n)^{45}Sc reaction at 68 MeV with a metallic 0.8 mg/cm^2 target over their kinetic energy and scattering angle. In all, 2 million events have been calculated and the contour lines present the number of recoils per 0.2° and 174 keV angular and energy intervals in steps of 100 recoils, with 800 recoils in the maximum of the distribution.

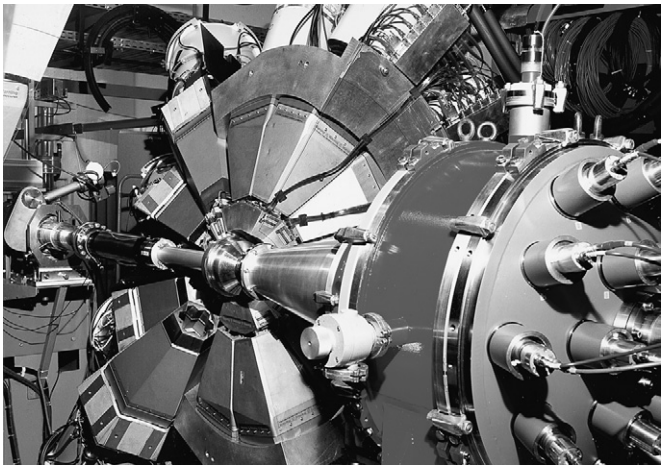

Fig. 6. Photograph of RFD in conjunction with the EUROBALL IV array on line with the VIVITRON tandem accelerator at IReS (courtesy of Ch. Munch, IReS, Strasbourg). The beam enters from the left. The right half of EUROBALL IV is pulled back, showing the target chamber in front of the Clover and Cluster γ-ray detectors, connected with the RFD tank by the conical chamber. The tank of RFD, replacing the EUROBALL IV tapered Ge-detectors, is seen to the right. Several photomultiplier bases sticking out of the back cover of the RFD tank are also visible.

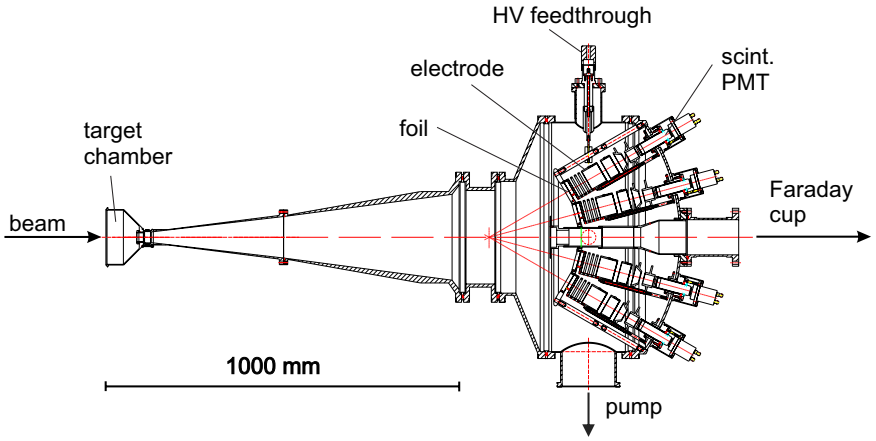

Fig. 5. Vertical cut through RFD used with the EUROBALL IV array on line with the VIVITRON accelerator at IReS in Strasbourg (see text for explanation).

is calculated as the sum of the solid angles of the individual elements. At the distance of 1350 mm it is 19.4 msr. At the shorter distance of 1000 mm, RFD covers the angular interval from 2.4° to 9.0° with the solid angle of 36.3 msr.

Fig. 7. Photograph of the 18 cylindrical detection elements of RFD (courtesy of Ch. Munch, IReS, Strasbourg). The first electrodes of the elements mounted in an aluminum plate under high electrostatic negative potential are seen to the left. The electron-emitting foils are removed to show the inside of elements. In the center of the picture, aluminum electrodes isolated from each other by lucite insulators are seen. The photomultipliers with the scintillators are not mounted in the holes of the RFD back cover seen to the right.

A turbomolecular pump is connected to the lower port, and the high-voltage feedthrough for electrodes is mounted in the outlet on the top, of the RFD tank.

Photographs of RFD coupled to EUROBALL IV and its array of 18 detection elements are shown in Figs 6 and 7.

3.3. Secondary-electron emissive foil

We have already pointed out that RFD has to detect down to very slow heavy nuclei in the presence of a very high rate of scattered beam particles. Therefore, a detection mechanism that gives signals with a height proportional to the electronic energy loss of the nucleus or number of secondary electrons knocked out from a very thin foil by recoiling ions is favorable, as described in Section 2.

Following Bohr, the process leading to the ion energy loss can be considered as caused by two extremely different types of collisions, referred to as distant and close collisions [11]. The distant collision leads to the production of low-energy secondary electrons with isotropic angular distribution around the beam axis. The energy spectrum of the electrons has been measured for 500 keV protons bombarding thin carbon and aluminum foils [11]. It was demonstrated that about 75% of the total number of electrons emitted have an energy below 20 eV. The secondary electrons are emitted from the entrance and the exit surfaces of the foil. The ratio of the secondary electrons that are emitted in forward and backward directions depends on the mass of the ion. For heavy ions, as in our case, about 2/3 of the electrons are emitted in the forward direction [11].

The escape depth of such low-energy secondary electrons is about 1.5 nm [11]. Because of that small escape depth, the total electron yield is only sensitive to events in the first few atomic layers at the beam entrance and exit surface of the solid. Recoils that are stopped inside of the Mylar foil cannot be detected by the secondary electron emission. Moreover, for slow heavy nuclei the electronic energy loss drops with decreasing energy. Therefore, the foils for slow

Table 1
Electronic energy loss $(dE/dx)_{el}$ of ions representative for beam, fission products and heavy evaporation residues passing through the 0.8 μm Mylar and then 20 nm aluminum of the secondary electron emitting foil [15] for typical ion energy E_{in} at the entrance of the foil

Ion	E_{in} (MeV)	$(dE/dx)_{el}$ (MeV)/(mg/cm^2) Mylar	E_{out} (Mylar) (MeV)	$(dE/dx)_{el}$ (MeV)/(mg/cm^2) Al	E_{out}(Al) (MeV)
^{4}He	30	0.22	30.0	0.17	30.0
^{16}O	100	3.86	99.6	3.04	99.6
^{40}Ar	200	17.10	198.1	13.39	198.0
^{96}Zr	100	54.70	93.9	35.52	93.7
^{124}Sn	100	62.59	93.0	38.92	92.8
^{208}Pb	5	15.48	2.2	8.86	2.1
	10	18.78	7.2	13.46	7.1
	20	24.41	16.8	17.03	16.7
^{226}Th	5	15.70	2.0	8.70	1.9
	10	19.16	7.0	13.58	6.9
	20	23.89	16.7	17.02	16.6

Calculated energies at the exits of Mylar foil E_{out}(Mylar) and aluminum layer E_{out}(Al) are also given.

heavy-ion detection should be as thin as practically feasible. Mylar foils between 2.0 and 0.5 μm of thickness and 56 mm of diameter have been used. The exit surface of the foils was covered by aluminum of 20 nm thickness to ensure a uniform electrical potential of the foil under high-voltage tension applied for acceleration and focusing of the secondary electrons onto the scintillator (Section 3.4). Because of the small escaping depth, the secondary electrons are preferentially emitted from the aluminum layer. The slowest ions that have been detected so far by RFD are thorium nuclei of 6 MeV and below (Section 4.1.1).

Table 1 lists the calculated electronic energy loss [15] in 0.8 μm Mylar foil and 20 nm aluminum layer for some ions that represent beam particles, fission products and evaporation residues. According to Section 2, one can expect that the total number of secondary electrons emitted from the foil by heavy mass recoils should be from 100 to 400. The corresponding pulse height induced by forward electron emission and 20 kV accelerating voltage should lie in the energy interval from 1 to 4 MeV. It turns out that the expected pulse height is largest for fission products and almost equal for an argon beam and slow heavy recoils. These estimates have been confirmed by measurements of the number of secondary electrons produced by the recoiling nuclei actually detected in RFD as described in Section 3.6.

3.4. Acceleration and focusing of secondary electrons

A schematic drawing of one of the 18 identical RFD detection elements is shown in Fig. 8. Its primary task is to accelerate and focus all secondary electrons that are emitted from the foil onto the scintillator, independent of the position where the ion hits the foil. As the kinetic energy of the emitted electrons is negligible (20 eV) compared to the energy achieved after acceleration (20 keV), this poses no principal difficulty. But while in usual beam optics particles are limited to a narrow range around the axis, electrons originating at the edge of the aperture of the optical elements are also treated here. The calculated ion optics [16], as presented in Fig. 8, gently guide the electrons from that edge towards the axis by an increasing axial electric field generated by the first 4 ring-shaped electrodes. A decisive influence for the acceptance of the electrons right from the outer radius of the foil is exerted by the position of the foil relative to the first equipotential ring, in which it is mounted. Trajectory calculations [16] demonstrate that the foil has to be 1 mm inside the ring as shown in Fig. 8. A very thin aluminum layer of 20 nm thickness evaporated onto the exit surface of Mylar foil ensures a uniform electrical potential. The boundary conditions at the edge of the foil need the electric field lines to be perpendicular to the conducting surface, while a radial component of the field right behind the foil collects the electrons from the edge. The two long electrodes at 0 and −15 kV and the following conical electrode at −2 kV form a deacceleration–acceleration focusing lens. According to the calculations, all electrons are then focused within a diameter of 15 mm at the scintillator. The time-of-flight of the electrons through the detection element calculated at −20 kV is 5 ns, with a spread smaller than 100 ps.

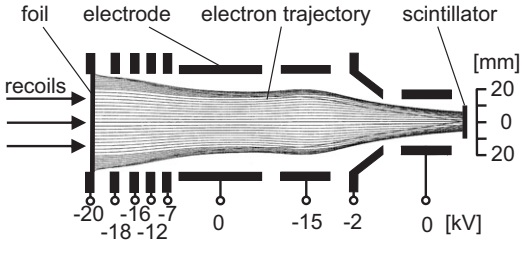

Fig. 8. Schematic drawing of the cylindrical detection element of RFD. The electrodes and their electrostatic negative potentials for the accelerating voltage $U = -20$ kV are shown. They accelerate and focus secondary electrons from the emitting foil at the left onto the scintillator at the right. Electron trajectories are calculated [16] for secondary electrons emitted from the foil with zero kinetic energy.

The focusing of the electrons emitted from the foil of 56 mm diameter onto a surface of about 15 mm diameter (see also Section 3.6) has several advantages. A small scintillator of about 3 mg mass might be used. Consequently, its sensitivity to γ-ray, neutron and electron background is very low. Also, smaller PMs can be applied; this is cheaper and makes the whole mechanical setup much simple. For the first model of RFD, scattered beam particles could directly hit a part of the scintillator of the 6 inner RFD elements. This was tolerable because of the small area of the scintillators, but the huge pulses from these hits were bothersome. Therefore the detection elements of the RFD model 2 are tilted away from the axis so that the small scintillators cannot be hit directly.

Electrons are also emitted anywhere inside the accelerating element due to other radiation or from rough spots of the material. If they are accelerated and reach the scintillator, they cause noise. This is much suppressed by the design as the trajectories of very few electrons that are emitted from other places than the foil will reach the scintillator. It was observed that the noise of the detection elements at the operating voltage could be reduced significantly by the conditioning procedure performed well ahead of measurements. In this procedure, the accelerating voltage was slowly raised in small steps up to −27.5 kV. The output of the PMs became noisier with each step and it was allowed to settle before the next one. After reaching the maximum value, the voltage was slowly lowered to the operating potential (usually −20 kV).

3.5. Scintillators and PMs

Scintillators and PMs are chosen for the detection of the secondary electrons emitted from the foil because they can handle very high counting rate and are sturdy and easy to use. Scintillators sum up the light generated by almost

simultaneously arriving secondary electrons, which means that the pulse height is proportional to the number of electrons as wanted. As the light output is proportional to the energy of electron, stray electrons that originate from other places than the foil with a lower electrostatic potential contribute less to the noise. Commercially available 10 μm thick Pilot U plastic scintillators in the Nuclear Enterprises technology with a very short decay time of 1.36 ns are used. The scintillator thickness is greater than the range of 20 keV electrons (about 6 μm) to assure full absorption of electrons at this energy in a plastic absorber. The scintillators are also quite resistant to radiation damage. Around 10^8 electrons per second deposit 20 keV each in the scintillator. The mass of the scintillator is only about 3 mg and the absorbed dose in one day—the characteristic time scale of an experiment—is 10^4 Gy. The scintillators are attached to photocathode windows of the PM tubes with silicon grease and held down by aluminum rings that also define the scintillator sensitive area.

The PMs are found to be a critical part of the system. Their gain decreased significantly during the course of experiment due to the high average load, changing often by orders of magnitude (''fatigue'' phenomenon in PM). It turns out that the PM operation is much more stable if its gain is kept rather low and instead fast electronic amplifiers are used in addition. Therefore, every one of the 18 individual RFD scintillation detectors is based on an 8-stage PM PHILIPS XP2962 (instead of a 11-stage PHILIPS XP2982 used in the RFD model 1) with a base manufactured by HMI (Berlin). A positive high voltage is applied to the anode, necessitating capacitive coupling of the signal pulses, but the mechanical construction is much simpler with the photocathode and consequently the PM tube kept on ground potential. To provide good gain stability at high counting rate, the PMs operate at a low anode potential of about +700 V, well below the recommended voltage (+1000 V). Although the timing properties of the PM tube are not optimized at such low voltage, other properties such as linearity or signal-to-noise ratio are not appreciable changed (see Section 3.6). In addition, emitter followers for the last three dynodes are used in the resistive voltage dividers.

The PM tubes are glued with epoxy into aluminum flanges that are the vacuum seals into the back cover of the detector chamber. The PM tubes are screened from possible stray magnetic field by the PHILIPS mu-metal shields in the form of cylinders extended beyond the photocathode plane and connected to the tube ground potential.

Because the fast negative signal of low amplitude (about 20 mV) from the anode is used both in time and pulse-height measurements, it is amplified by a fast preamplifier without any degradation of signal rise time and then by the LeCroy 612 Fast Amplifier, with a total electronic gain of 100 (see also Section 3.7.1). The fast preamplifier built in IFJ PAN (Krakow) is based on the low-distortion, 1 GHz current feedback AD 8009 amplifier.

3.6. Tests with a ^{252}Cf fission source

A thin fission source of ^{252}Cf was used for the development and tests of RFD and its data-acquisition system prior to in-beam experiments. The fission fragments, very roughly nuclei of mass 100 and 100 MeV of kinetic energy, are similar enough to the evaporation residues and well suited to test the detector. Also, about 10 γ-rays are emitted per fission event. Therefore, coincidences between fission products and γ-rays can be easily measured with RFD and a simple γ-ray detector.

Both the individual RFD detection elements in a separate chamber and the complete RFD setup were tested with a ^{252}Cf source in coincidence with large NaI(Tl) scintillation counters, like the $3'' \times 5''$ NaI(Tl) Harshaw spectrometer. A data-acquisition system with dedicated software was built to acquire data for creating and analyzing single and coincidence spectra in one- and two-dimensional modes as described in Section 3.7.2. Below,

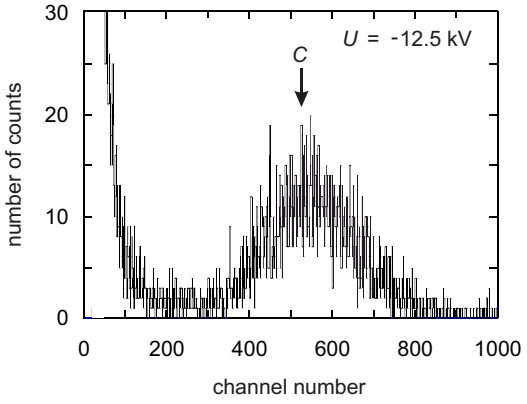

Fig. 9. Pulse-height spectrum of the secondary electrons from 0.8 μm thick aluminized Mylar foil illuminated by a ^{252}Cf fission source, measured without any coincidence requirement by one detection element of RFD with the electron accelerating voltage $U = -12.5$ kV and the PM operating at +700 V. *C* marks the centroid of the pulse-height distribution.

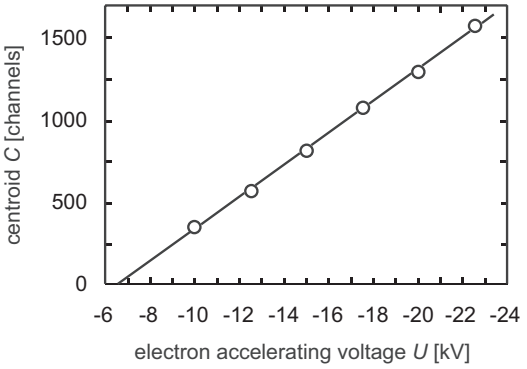

Fig. 10. Centroid *C* of the pulse-height distribution of the secondary electrons emitted from 0.8 μm thick aluminized Mylar foil bombarded by fission fragments of a ^{252}Cf source as function of the electron accelerating voltage *U* of the RFD detection element. The dependence is linear as expected, but with a bias of −6.5 kV (see text).

results of three selected tests of the main properties of RFD with a ^{252}Cf source are presented.

Fig. 9 shows the pulse-height distribution of fission fragments as measured by one RFD detection element at a low electron-accelerating voltage of $U = -12.5$ kV without requiring a coincident γ-ray. The PM tube operated at +700 V, much below the recommended voltage for better gain stability at high counting rate as discussed in Section 3.5. The peak is wide but clearly separated from the exponentially falling background. The spectrum was measured also as a function of the electron acceleration voltage U. As expected, the centroid C of the peak moves linearly with U (Fig. 10), clearly demonstrating that PM can operate below the recommended voltage without changing its general performance. Surprisingly, a large bias of −6.5 kV was found. This bias has always been seen for all detection elements, varying between −5 and −10 kV, but its origin has not been understood yet.

In the second test, we determined the average number of secondary electrons emitted from the aluminized Mylar foil illuminated by fission fragments from a ^{252}Cf source. The test was based on a simultaneous measurement of pulse-height spectra of fission fragments and 6.1 MeV α-particles from ^{252}Cf by the RFD detection element with a thick scintillator, as described in detail in Ref. [14]. The centroid of the secondary electron peak was expected at a position that was determined by three factors: (i) the average number of electrons emitted, (ii) the light yield for a plastic scintillator excited by electrons and (iii) the acceleration voltage. The corrections for a fraction of normally incident electrons, which were backscattered from the scintillator surface, and for the just-mentioned bias of the accelerating voltage should also be taken into account. On the other hand, the position of the α line in the spectrum was defined by the energy of α-particles and the light yield of plastic scintillator for this particle at 6.1 MeV. Therefore, the average number of electrons could be calculated from the ratio of peak positions for secondary electrons and α-particles if the ratio of the light yields for α-particles and electrons was determined experimentally. A 1 cm thick Pilot U scintillator irradiated by γ-rays from sources of ^{133}Ba, ^{137}Cs and ^{22}Na showed the Compton edges at electron energies of 207, 478, 341 and 1061 keV well enough for a crude calibration of the pulse-height spectrum in electron energy. The position of α line in a spectrum was measured and determined to correspond to an electron energy of 740(100) keV. This allowed establishing the experimental ratio of light yields for α-particles and electrons as 0.121(15). In consequence, the average number of secondary electrons emitted from the aluminized Mylar foil by fission fragments from ^{252}Cf was found to be 270(70). According to Rothard [11] (Section 2), in this case, 410 electrons were expected in total and about 270 electrons emitted in the forward direction. This agreed surprisingly well with the measurement.

The third test verified the results of the calculation, showing that secondary electrons emitted from any point of the Mylar foil hit the scintillator within a circle of 15 mm in diameter. The foil was uniformly bombarded with fission fragments from a ^{252}Cf source, while the scintillator was covered with diaphragms of varying diameters. Fig. 11 shows the measured counting rate of the RFD detection element as a function of the diaphragm diameter d. For $d \geqslant 15$ mm the counting rate is constant, proving that electrons from the whole area of the foil are guided to the scintillator within the calculated diameter of 15 mm.

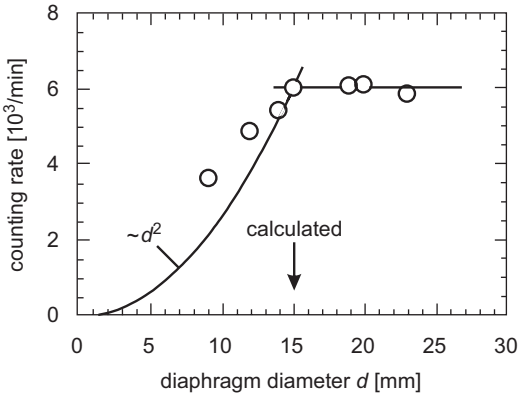

Fig. 11. Counting rate of one RFD detection element illuminated by fission fragments from a ^{252}Cf source in a function of diameter d of diaphragm mounted on a plastic scintillator of the detector. A constant counting rate for $d \geqslant 15$ mm indicates that the measured diameter of the secondary electron focus is equal to this value in very good agreement with calculations.

3.7. Electronics and event handling

3.7.1. Electronics for in-beam experiments

In this section, we present the recent version of the RFD electronics as used within the last period of the RFD campaign at the EUROBALL IV array on line with the VIVITRON accelerator at IReS in Strasbourg.

A block diagram of the electronics in Fig. 12 demonstrates the application of the time-of-flight technique for filtering of evaporation residues from a huge background of the scattered beam particles using RFD in conjunction with EUROBALL IV. The system presented here offers also a possibility to measure both the time-of-flight and the pulse height for each individual recoil detected in RFD in coincidence with the γ-event of selected fold formed by EUROBALL IV synchronously to the beam pulse signal from the accelerator pulsing system. The electronics scheme has been assembled using commercially available modular electronics of the NIM and VME standards manufactured by CAEN, GSI, LeCroy and ORTEC. However, to perform special tasks, purpose-built electronic modules have been developed by HMI (Berlin) and IFJ PAN (Krakow).

The pulsed beam, when used, should have a repetition time slightly longer than the time-of-flight of the slowest evaporation residues. The pulses from the PMs of RFD detection elements (18 PM PHILIPS XP2962) are first

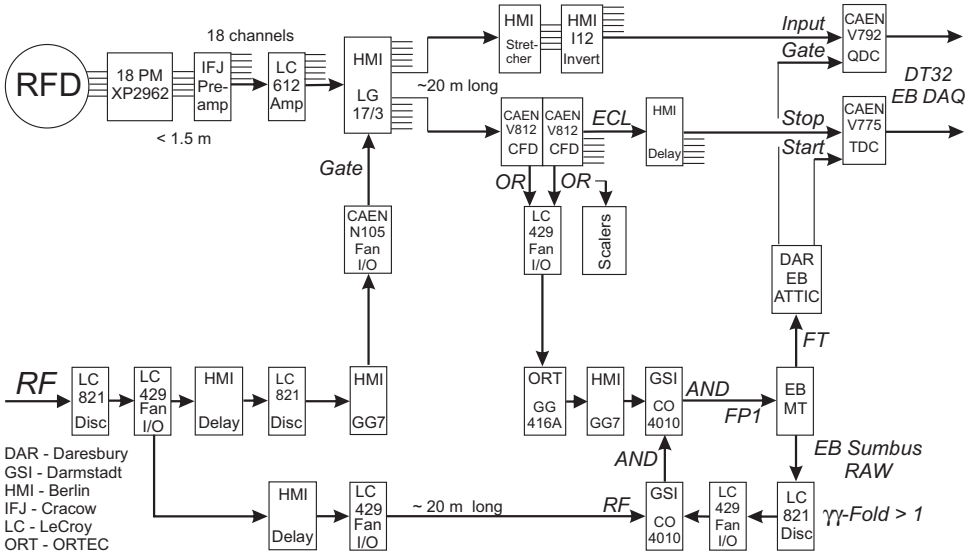

Fig. 12. A block diagram of the electronics for measurements of time-of-flight and pulse height of recoils in coincidence with γ-rays using RFD and the EUROBALL IV spectrometer on line with the VIVITRON accelerator at IReS (see text for explanation).

amplified by the fast preamplifier (IFJ Preamp) and the LeCroy 612 Fast Amplifier (LC612 Amp) and then fed to fast linear gates (HMI LG17/3)—the key elements of the system—that are opened and closed strictly periodically with the time reference to the RF beam pulse signal. The task of the gates is to eliminate the scattered beam particles that arrive at a well-defined time (see Fig. 13). The allowed time range, during which the gate is open, covers the time interval when the evaporation residues arrive. In a typical fusion–evaporation reaction, the inner detector elements are each hit as noted already, by about one scattered beam particle per beam pulse. Standard electronics would give a dead time of some 100 ns, and evaporation residues would be lost almost always. The fast linear gates and the preceding amplifiers (IFJ Preamp and LC612 Amp) are located close to the detector and connected with short cables (~1 m). With this scheme, it is possible to handle the huge counting rate of scattered beam and reduce it behind the gates to a low enough level that the following standard electronics can stand.

The remaining electronics modules can be placed at a long distance from the target, in the counting area, connected by coaxial cables about 20 m long. A time signal is generated for all elements individually by constant fraction discriminators (CAEN V812 CFD). The OR logic signal derived from CFD provides information that an individual RFD detection element has been hit by one recoil. This is a "valid recoil event". The system is not protected against multiple hits, when two or more detector elements are fired at the same time. However, the rate of multiple hits is usually kept below 3% of the total RFD rate and the sorting program rejects such events off-line. The pulse-height information is stored by means of linear stretchers (HMI Stretcher) in the processing chain of pulse-height measurement for about 1 μs until a logical decision has been made on the validity of the event.

EUROBALL IV provided a "valid γ-event" signal. This was a prompt coincidence of at least two prompt (relative to the beam pulse) Ge-detector signals. We found out that a fold value even as low as 2 could be meaningful in the measurement of γ-recoil coincidence spectra. γ-Events of a proper fold were selected by a discriminator (LC 821 Disc) analyzing the signals provided by the EUROBALL IV Sumbus Raw output of the EUROBALL IV Master Trigger card (EB MT). The γ-event of a selected fold (γγ-Fold > 1) was synchronized in time with the RF signal (GSI CO 4010 AND) being in phase with the beam pulse that ensured these γ-rays to be prompt. A coincidence of this valid γ-event with the valid recoil event (GSI CO 4010 AND) constituted a "valid event" signal. This information, that RFD and EUROBALL IV detectors were in true time coincidence, was fed to the Front Panel 1 (FP1) of the EUROBALL IV master trigger (EB MT). The master trigger performed the AND functions for the shaped and delayed sumbus and the FP1 signals and provided the fast trigger (FT) logic signal. The fast trigger signal forced the EUROBALL IV ATTIC module (DAR EB ATTIC) to generate the common start signal for the TDC (CAEN V755 TDC) that measured the time-of-flight and the gate signal for the QDC (CAEN V792 QDC) for sampling the stretched pulse heights of recoils.

The valid event signal fed to the input FP1 of the master trigger started the conversion for the signals from the γ-ray detectors and afterwards provided the fast read-out of the TDC and ODC converters with the VME processor. Then the data were delivered to the DT32 bus for further processing by the EUROBALL IV data-acquisition system (DT32 EB DAQ) and stored event-by-event on a mass

storage device. Here, an event consisted of the pulse height and time-of-flight information from RFD and the γ-ray data from EUROBALL IV.

The counting rates of the RFD detection elements were monitored by scalers (Scalers) behind the CFDs for fast online check. Other significant signals, like "valid events", were also counted.

3.7.2. Electronics and software for off-beam tests

Computer-controlled CAMAC modules with ECL logic are used to process in parallel the time and pulse-height signals from the RFD detection elements in test experiments off-beam with a ^{252}Cf fission source (see Section 3.6). A special software named EURYDICE has been prepared to control the CAMAC electronics and to collect data [17]. EURYDICE is written in C++ language in a fully object-oriented way and runs under the Window^{TM} operating system on the dedicated PC. The EURYDICE software models the hardware configuration by using classes such as "CAMAC crate" or "CAMAC block". A CAMAC block, for example, corresponds to an abstract type of a CAMAC hardware module. The user of the EURYDICE software sees on the screen a picture of the hardware, i.e. the crates with modules in the appropriate slots. The user can interactively define the software that corresponds to the hardware by specifying which type of module is in a given slot of the crate. He can also read out and adjust the settings of all CAMAC modules, like thresholds of the CFDs or delays, using dedicated dialog windows. The configuration and all settings can be saved for later use.

The EURYDICE software is able to acquire data in two modes. The "single mode" collects the set of single spectra of all the TDC and QDC channels. In this mode of acquisition, the data are synchronously taken directly from the modules via the CAMAC readout. In the "event-by-event" mode, the data from the TDC and QDC modules are read event-by-event via FERA readout into a specially built FDT32 CAMAC module [18]. This module buffers the data and then transfers them to EURYDICE for construction and analyses of one- and two-dimensional spectra.

4. Performance of the detector

4.1. Measurements with pulsed beam

4.1.1. Filtering of evaporation residues and detection efficiency

The ability of RFD to filter evaporation residues from other reaction products can be clearly demonstrated in the heavy mass region where fission process and Coulomb excitation of target nuclei dominate. The reaction of the 141 MeV ^{28}Si pulsed beam with 430 ns repetition time on a 0.7 mg/cm^2 thick ^{175}Lu target is selected as a representative example. According to the CASCADE code calculation [14], the total fusion cross-section is 100 mb, but the fission of a compound nucleus is almost 30 times more probable than the particle evaporation. In particular, the calculated cross-section for ^{175}Lu(^{28}Si,4n)^{199}At reaction considered in Section 3 is only 120 μb [14], in good agreement with the measured value of 100 μb [8].

The γ-rays were detected by 14 Compton-suppressed HPGe-detectors and 1 LEPS detector of the GAREL+ set-up (GAmma+Recoil+ELectron+…) [8] in coincidence with any recoil detected by RFD. The total photopeak efficiency of the GAREL+array was 1.5%. The recoil detector was placed at a distance of 1340 mm from the target covering the angular range from 1.8° to 6.6°. The requirement for a valid event was a coincidence of RFD with at least two Ge-detectors. Fig. 13 shows a two-dimensional plot of the pulse height versus time-of-flight measured by one RFD detection element for recoils emitted from the target. The beam pulses are cut out in narrow time intervals around 50 ns at the left of the figure and around 480 ns to the right. Region A contains the Landau-tail of the beam pulse and fission products. It might be noted that, in contrast to the evaporation residues and the beam, fission products are emitted nearly isotropic in the laboratory frame. Requiring a coincidence with any kind of nucleus in a very narrow forward cone reduces substantially, therefore, the background from the fission. Region B is due to fusion reactions on target impurities of chromium, manganese and iron, as verified by the presence of characteristic γ-ray lines in the measured γ–γ-recoil coincidence spectrum. These impurities are likely from rolling the target between stainless steel rollers. The region C contains ^{175}Lu recoils from Coulomb excitation of the lutetium target. The heavy evaporation residues of interest are in the region D, very well separated from other reaction products. The hardware threshold of the constant-fraction

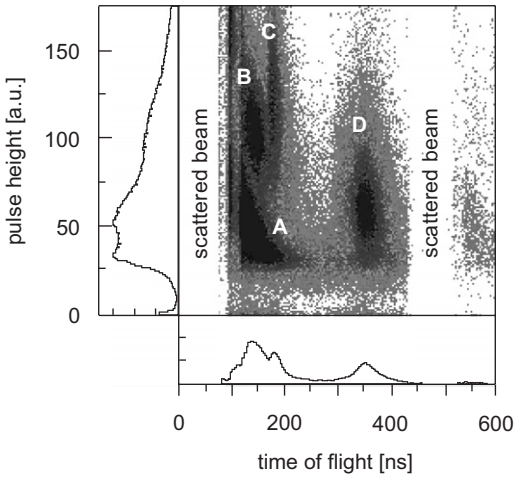

Fig. 13. Two-dimensional plot of a pulse height vs. time-of-flight of recoils from the reactions of pulsed ^{28}Si beam at 141 MeV with a 0.7 mg/cm^2 thick ^{175}Lu target measured with RFD at a distance of 1330 mm from the target at the GAREL+setup. Very good separation of evaporation residues (D) from other reaction products (A–C, see text for explanation) is clearly seen. Total projections on the pulse-height axis and on the ToF axis are also shown. The scattered beam particles are cut by fast linear gate.

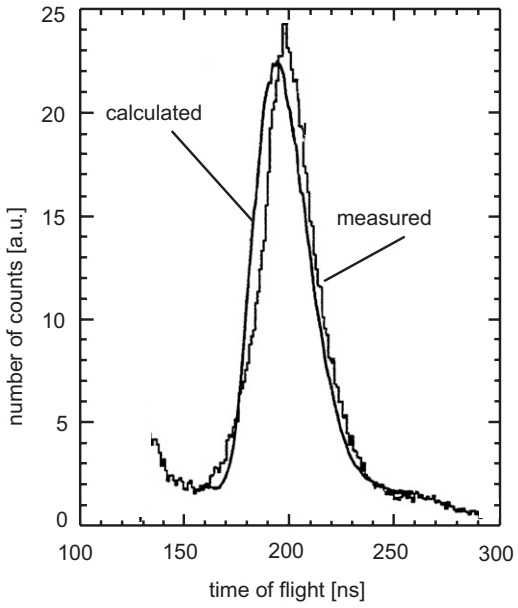

Fig. 14. Time-of-flight distribution of ^{199}At nuclei from the reaction of pulsed ^{28}Si beam at 141 MeV with a 1.0 mg/cm^2 thick ^{175}Lu target measured by RFD placed at a distance of 733 mm from a target. The histogram gives the measured spectrum. The smooth line shows the calculated distribution accounting for the energy spread from the recoil of the neutrons and energy loss straggling.

discriminator is evident as the rapid change in counting rate at a pulse height around 25 units. The figure shows also that the noise extends to roughly this amplitude and obscures little the distribution of the wanted nuclei. The total projections on the pulse-height axis and on the time-of-flight axis are also shown.

The Monte Carlo TRIMTRANS code calculations reproduce in good agreement with measurements the important features of investigated reactions and the experimental setup, like time-of-flight distribution of recoils and the detection efficiency of RFD. Fig. 14 shows a calculated time-of-flight spectrum of ^{199}At nuclei from the reaction of ^{28}Si at 141 MeV on a ^{175}Lu target of 1 mg/cm^2. It follows quite well the experimental time distribution measured by RFD coupled with a γ-ray detector array at a distance of 733 mm.

The detection efficiency of RFD is determined as the ratio of intensity of a selected γ-ray line in a γ-ray spectrum gated by evaporation residues to the intensity of this line in a spectrum measured without requirement of coincidences with recoils of interest. According to the definition, the RFD efficiency can be measured only in such cases, in which a selected γ-ray line can be distinguished from a background in a spectrum not gated by recoils. This condition makes the efficiency measurement for the ^{175}Lu(^{28}Si,4n)^{199}At reaction rather difficult because, in the not-gated spectrum, γ-ray lines from the (4n) evaporation channel are obscured by a huge fission background. Therefore, the efficiency of the detector was measured for the similar ^{154}Sm(^{28}Si,4n)^{178}Os reaction at 141 MeV and a 0.7 mg/cm^2 samarium target, but with a cross-section about 100 times higher than for the ^{199}At nuclei. In this measurement, RFD was mounted at a shorter distance of 1160 mm from the target, covering the angular interval from 2.0° to 7.9°. Intensities of several prominent γ-ray lines from de-excitation of the ^{178}Os nucleus in the γ-ray spectrum and the γ-recoil coincidence spectrum were evaluated and the mean efficiency was determined as 35(5)%. The measured efficiency agrees well with the value of 33% calculated by the TRIMTRANS code.

The ability of filtering of weekly populated evaporation residues from a very intense background of other reaction products with high efficiency has allowed for the first time to perform spectroscopy investigations of the mid-shell ^{186}Pb and ^{188}Pb nuclei [7].

4.1.2. Detection of very slow recoils

As it was described in Section 3, recoiling heavy ions to be detected by RFD have to pass through a thin foil to knock out secondary electrons. This requirement would limit the application of RFD for spectroscopic studies of very heavy nuclei, if they were produced in a fusion–evaporation reaction with very low velocity. In order to overcome this difficulty, we have applied very thin, 0.8 μm aluminized Mylar foils allowing detecting heavy mass recoils with kinetic energy as low as 6 MeV. The ^{220}Th nuclei with a kinetic energy of about 6 MeV produced in a

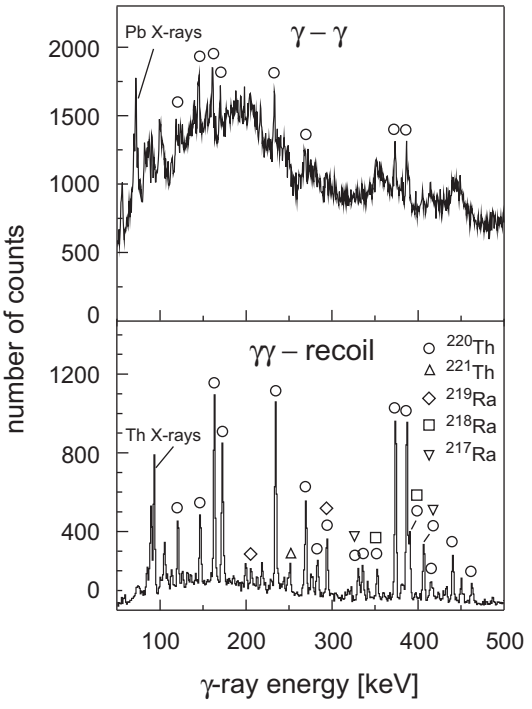

Fig. 15. Total projection of γ–γ coincidence spectrum from the reaction of pulsed ^{16}O beam at 92 MeV with a 250 μg/cm^2 thick ^{208}Pb target measured by the GAREL + Ge-detector array (top panel) and the spectrum gated in addition by evaporation residues recoiling to RFD (bottom panel). The most intense γ-ray lines from various fusion–evaporation channels as well as X-ray lines from the target and main reaction products are indicated. Spectra are not normalized.

reaction of 92 MeV ^{16}O with 250 μm thick ^{208}Pb target were used to test RFD with Mylar foils of this thickness. Fig. 15 shows the total projection of the γ–γ coincidence spectrum (upper panel) and the γ–γ-recoil-gated spectrum (lower panel) from the investigated reaction. The upper spectrum without RFD coincidences is obscured by an intense fission background and only a few γ-ray lines from fusion–evaporation reactions are seen. The X-rays from the Pb-target are prominent. The lower panel shows clearly that the requirement of RFD in coincidence gives the spectrum with the peak-to-background ratio improved by one order of magnitude and γ-ray lines from fusion–evaporation residues only. The Pb X-ray lines are completely suppressed, and now the X-rays from main reaction products (Th nuclei) can be seen.

Thinner aluminized Mylar foils of 0.5 μm thickness have become available in the meantime, making possible spectroscopic studies of even slower and very heavy nuclei, with a kinetic energy as low as 5 MeV.

4.1.3. Correction of Doppler broadening

It is well known that thin-target γ-ray spectroscopy experiments, especially for light mass nuclei, suffer a significant Doppler broadening of γ-ray lines. The observed broadening is related to the spread in velocity and angle of recoils and to the opening angle and position of the γ-ray detectors. Fig. 16 (top panel) illustrates the loss of energy resolution due to the Doppler broadening in the γ-ray spectrum from the reaction of ^{18}O beam at 67 MeV with a 0.8 mg/cm^2 thick, metallic ^{30}Si target. Indeed, as shown in Fig. 4, the distribution of ^{45}Sc recoils produced in the main (p2n) evaporation channel of the investigated reaction is very wide both in scattering angle and in recoil velocity. In order to minimize the effect of the uncertainty in the angle of γ-ray emission, the spectrum of Fig. 16 was measured by one Ge-crystal of the EUROBALL IV Cluster detector with the half-opening angle of 4.5°, positioned at 156°. In addition, the Doppler shift was corrected for using the mean velocity ($v/c = 0.028$) of the recoiling nuclei. Nevertheless, the large uncertainty in the velocities of recoiling nuclei, equalling about 30% for ^{45}Sc nuclei, still broadens measured γ-ray lines significantly, resulting in the relative energy resolution of about 2% for 1500 keV [19].

In stark contrast to this, narrow γ-ray lines with the relative energy resolution of 0.3% at 1500 keV result (Fig. 16, bottom panel) if the Doppler shift of each γ-ray is corrected for using the measured velocity vector of the individual nucleus from which it was emitted. The magnitude of the velocity is given by the time-of-flight, whereas the recoil direction is determined by the RFD detection element that has been hit.

The relative uncertainty of about 1%, which can be usually achieved in ToF measurement for nuclei recoiling with the velocity of few percent of the light velocity, leads to the Doppler broadening of γ-ray line comparable with the intrinsic resolution of Ge-detector or—in most cases—significantly smaller. The small opening angle of the individual detection element (about 20% of that of the Ge-detector) contributes at most 2% to the broadening of the γ-ray line. Therefore, in this case, Doppler broadening of the γ-ray line is almost fully determined by the finite opening angles of γ-ray Ge-detectors. This is illustrated in Fig. 17, where the full width at half maximum (FWHM) of γ-ray line corrected event-by-event for the Doppler shift is plotted vs. γ-ray energy for slower ($v/c = 0.04$) and faster ($v/c = 0.05$) recoils: ^{47}V and ^{49}Cr from the 125 MeV ^{28}Si + ^{28}Si reaction and ^{41}Ca from the 125 MeV ^{28}Si + ^{16}O reaction on silicon target impurities, respectively. As expected, this function is linear and different slopes of the two straight lines result from different velocities of

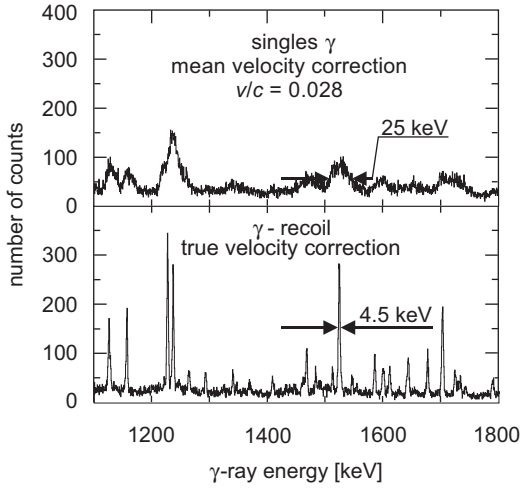

Fig. 16. Part of the γ-ray spectrum from the reactions of pulsed ^{18}O beam at 67 MeV with a 0.8 mg/cm^2 thick, metallic ^{30}Si target with Doppler corrections for the mean velocity ($v/c = 0.028$) of the recoiling nuclei (top panel) and with the correction for the true recoil velocity measured for each recoil by RFD (bottom panel) [19]. The spectrum was measured by one Ge-crystal of the EUROBALL IV Cluster detector with half-opening angle of 4.5°, positioned at 156°.

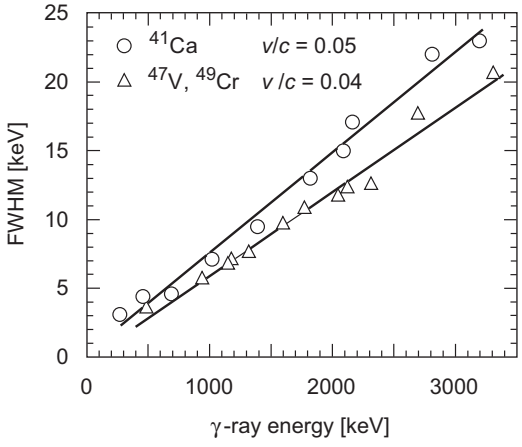

Fig. 17. The full width at half maximum (FWHM) of γ-ray line corrected for Doppler shift using the measured recoil velocity vector as a function of γ-ray energy. The experimental results are shown for evaporation residues recoiling with different velocities: ^{47}V and ^{49}Cr from the 125 MeV ^{28}Si + ^{28}Si reaction with $v/c = 0.04$ and ^{41}Ca from the 125 MeV ^{28}Si + ^{16}O reaction on silicon target impurities with $v/c = 0.05$.

recoils: the slope of the line plotted for faster recoils is greater than for slower ones.

The significant improvement in energy resolution has allowed spectroscopy of $f_{7/2}$ nuclei in the Ca-region [20–23] that was difficult or even impossible before. Also, superdeformed bands and their linking transitions to states of normal deformation could be found in the ^{61}Cu and ^{63}Cu nuclei [24]. This experiment is an example of combining of two ancillary detectors: RFD and the 4π charge particle detector EUCLIDES [9] with the EUROBALL IV array.

4.1.4. Evaluation of lifetime of excited states

The Doppler shift attenuation method (DSAM) is often applied to determine lifetimes of excited states in the femtosecond range by analyzing γ-ray line shapes. However, if the velocity distribution of the recoiling nuclei is very wide, as in the cases described here (Sections 3.1 and 4.1.3), an uncertainty in the velocity determination enlarges the Doppler broadening of γ-ray lines significantly and the DSAM becomes impractical. Therefore, in order to reduce the spread of compound nucleus velocity, the use of very thin targets is required [25]. In addition, employment of 4π charge particle detectors to reconstruct the initial velocity vectors of the residual nuclei can be advantageous [2,26]. The application of RFD, which measures precisely the velocity vector of every individual recoil, allows evaluating very short lifetimes of highly excited states also in such cases with more ease and precision. The Doppler shift of the γ-ray line can be corrected exactly, if the γ-ray is emitted behind the target where the recoiling nucleus has already well-defined velocity. When a short-lived excited state decays partly or entirely inside the target, the velocity vector of the nucleus changes before it is measured. The Doppler correction is then "wrong" and characteristically broadened lines result.

Three γ-ray lines from the reactions of the 68 MeV ^{18}O pulsed beam with 0.8 mg/cm^2 thick ^{30}Si target from a single EUROBALL IV Ge-detector placed at a backward angle are presented in Fig. 18. The bottom part shows a narrow line, as the sum of lifetime and feeding time of the excited state is long compared with the transit time of nucleus through the target material. In the middle of the figure, the lifetime and the transit time are almost equal, as indicated by the like areas of the narrow part and the tail of the line. Finally, the upper panel shows a case where the lifetime is short in comparison to the passage time.

This type of line shape analysis can be exploited in a qualitative way to determine the sequence of transitions, and it can also be used to quantitatively measure lifetimes of highly excited nuclear states. It can be proven that the ratio of area of the narrow part of the broadened γ-ray line to the total area of the line is expressed by the ratio of the lifetime of the state to the recoil transit time through a target material [27]. In this way, if the transit time of the recoil is known, the lifetime of excited, short-lived state can be estimated. Evaluated lifetimes of states considered here, with the transit time of recoils through a silicon target estimated as 400 fs [27], are shown in Fig. 18.

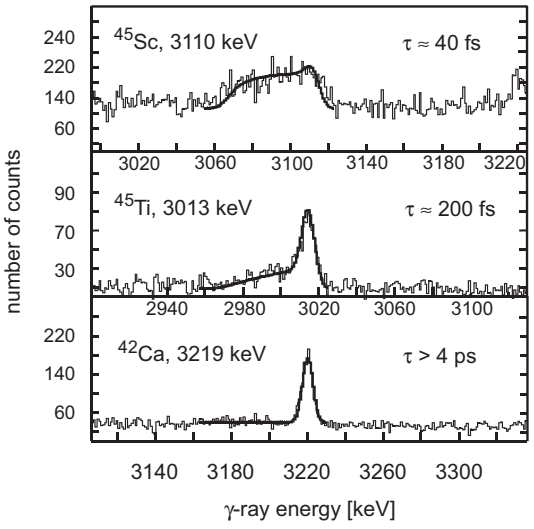

Fig. 18. Shapes of γ-ray lines in a recoil gated γ-ray spectrum from decay of excited states with lifetime longer (bottom), comparable (middle) and shorter (top) than a transit time of recoils through the target material estimated as 400 fs [27]. States were populated in the reactions of pulsed ^{18}O beam at 67 MeV with 0.8 mg/cm^2 thick, metallic ^{30}Si target. Recoil gated γ-ray spectrum was measured by the EUROBALL IV-RFD detecting system. Indicated in the figure are the approximate lifetimes τ of the decaying states extracted from the line shape analysis as described in the text.

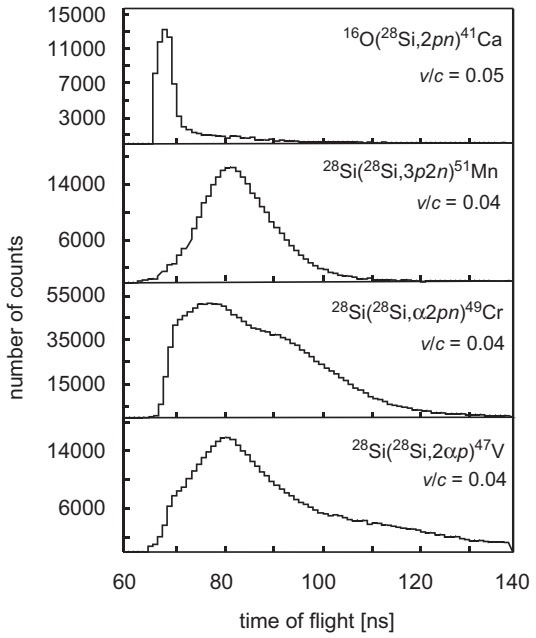

Fig. 19. Time-of-flight spectra for recoils emitted in various evaporation channels of the reaction of 125 MeV ^{28}Si on a 0.4 mg/cm^2 thick, metallic ^{28}Si target measured by the EUROBALL IV-RFD setup. For comparison, the ToF spectrum of recoils from the reaction 125 MeV ^{28}Si with ^{16}O impurities in silicon target is shown in the top panel. In the top and two bottom spectra, ToF distributions are cut off at the shortest flight times by the fast linear gate (see Section 3.7.1).

4.1.5. Identification of exit channels

Evaporation of different types and numbers of particles from the compound nucleus leads to significantly different time-of-flight spectra of evaporation residues, if the momentum of the particles is not too small relative to that of the compound nucleus. This is the case for charged particle emission up to the mass 60 region, where protons and α-particles are evaporated with energy around the Coulomb barrier. Thus, measurements of time-of-flight distribution of light evaporation residues can be used to some extent to identify the exit channels. Fig. 19 shows ToF spectra of evaporation residues from various exit channels of the 125 MeV $^{28}Si + ^{28}Si$ reaction measured with RFD coupled to EUROBALL IV, obtained by setting the coincidence gates on γ-rays from respective residual nuclei. In this example, the compound nucleus ^{56}Ni with the mid-target recoil energy of around 61 MeV leaves the thin target with the mean velocity of $v/c = 0.04$. The α-particles, protons and neutrons are emitted with mean kinetic energy of 15.5, 6.9 and 3.3 MeV, respectively [14]. The momentum of the α-particles is around 13% of that of the compound nucleus, while the momentum of protons and neutrons is roughly 4 times lower (4% and 3%, respectively). In consequence, the evaporation of three protons and two neutrons leads to wide but nearly symmetric ToF distribution of the ^{51}Mn residues (Fig. 19). If α-particles are emitted as in the two spectra at the bottom, the ToF spectrum becomes asymmetric and very wide. The dent in the spectrum for ^{49}Cr recoils is due to one α emission close to 90°, which pushes the nuclei to large angles out of the acceptance of RFD. The distribution of the ^{47}V residues for two evaporated alphas is also clearly wider than for one α emission. The top spectrum shows that reactions on lighter ^{16}O target impurities induce higher recoil velocity, and it can be easily identified by their difference in time-of-flight and narrow ToF distribution.

Fig. 19 clearly demonstrates that the time-of-flight spectra of light evaporation residues differ in shape so much that one can identify the exit channels. However, these ToF spectra overlap almost entirely and it is not possible to separate the γ-ray spectra from different channels by setting gates on the time-of-flight distribution of recoils.

For heavy evaporation residues, the ToF distributions do not differ significantly as the emission of light particles does not alter much the recoil velocity of the compound nucleus. For example, the momentum of protons and neutrons emitted in the 141 MeV $^{28}Si + ^{175}Lu$ reaction (Section 3.1) is 5% and 2% of the momentum of the compound nucleus, respectively. In consequence, RFD cannot identify different exit channels of the fusion–evaporation reaction in this mass region.

4.2. Measurements with continuous beam

In some cases, the basic concept of the detector makes possible the use of the continuous beam instead of a pulsing one to separate evaporation residue from the scattered beam. A good example is an asymmetric fusion–evaporation reaction of light projectiles on light–medium mass targets at bombarding energy slightly above the Coulomb barrier. In reaction of ^{18}O beam with ^{28}Si target at 106 MeV investigated here, the energy loss of evaporation residue of mass $A \sim 40$ passing through the Mylar foil of the RFD detection element is larger than for the scattered ^{18}O beam (see Section 3.3 and Table 1). In such case, evaporation residues may be fully separated by their pulse height from the scattered beam. The start signal for the recoil ToF measurement necessary for the Doppler shift correction can then be related to the trigger of the Ge-detector array, indicating that a true reaction event has occurred. Fig. 20 shows the two-dimensional spectrum of pulse height versus time-of-flight of recoils from the asymmetric fusion–evaporation reaction of the continuous ^{18}O beam on a 0.4 mg/cm^2 thick ^{28}Si target at 106 MeV measured with the EUROBALL IV-RFD setup. The EUROBALL IV trigger indicating that at least double γ–γ coincidence appeared was used as a start signal for the ToF measurement for individual recoils. Very good separation of recoils from the scattered beam particles is clearly seen. In the γ-ray spectrum, γ-ray lines corrected event-by-event for the Doppler shift with the true velocity vector revealed the same energy resolution for measurements with the continuous and the pulsed beams.

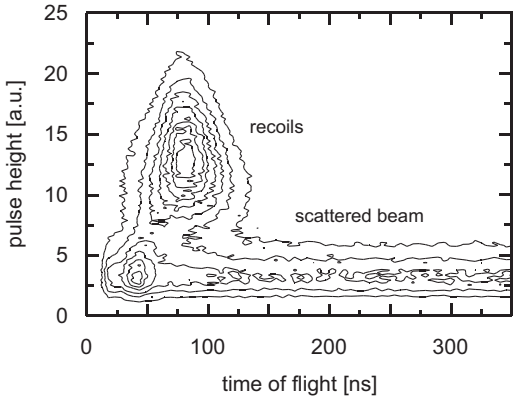

Fig. 20. Two-dimensional spectrum of pulse height versus time-of-flight of recoils from the asymmetric fusion–evaporation reaction of a continuous ^{18}O beam with a 0.4 mg/cm^2 thick ^{28}Si target at 106 MeV. The EUROBALL IV trigger indicating that at least double γ–γ coincidence appeared (γγ-fold ⩾2, see Fig. 12) was used as a start signal for the ToF measurement of individual recoils. Contour lines are plotted in steps of 290 counts with 2325 counts in the maximum of distribution.

5. Summary, comparison with other detectors and outlook

The high-efficiency detector of evaporation residues—the Recoil Filter Detector–has been designed, constructed and used in several in-beam γ-ray spectroscopy experiments. RFD measures evaporation residues emitted from a thin target into the narrow angular interval using a pulsed beam and the time-of-flight technique. The detection

scheme is based on the secondary electron emission induced by recoils from a very thin foil.

RFD, in conjunction with a highly efficient γ-ray detector array, like EUROBAL IV, and a 0.5 μm secondary-electron emitting foil is able to detect evaporation residues produced with a cross-section down to a few microbarns and a kinetic energy greater than 5 MeV. With the present design of RFD, an overall evaporation residue detection efficiency of about 30% is routinely achieved for light, medium and heavy nuclei. This could be increased to about 50% with careful matching of the RFD acceptance angle to the angular distribution of evaporation residues for the investigation reaction. The experimental RFD efficiency is comparable to that of gas-filled separators [28] and to the efficiency of the novel evaporation residue detector HERCULES for heavy recoils, as reported in Ref. [6]. However, HERCULES is particularly suitable for study of very asymmetric reactions and the detection efficiency as high as 59% was achieved recently for the $^{26}Mg + ^{198}Pt$ reaction at 128 MeV and a target thickness of 0.5 mg/cm^2 [29].

In the heavy mass region, RFD is able to filter a weak γ-radiation emitted by the evaporation residues from the competing background of fission. The requirement of a coincidence with evaporation residues significantly improves the peak-to-background ratio in the γ-recoil coincidence spectrum already with the fold as low as two. Although RFD in principle does not distinguish between various fusion–evaporation channels, the observed γ-ray lines in the γ-recoil coincidence spectrum can be correctly attributed to the unknown so far final nuclei. This was clearly shown in the spectroscopy investigation of the very neutron-deficient isotope ^{186}Pb with the OSIRIS-RFD setup [7]. The data with unambiguous mass identification of recoils obtained a little later by Baxter et al. [30] confirmed the assignment of the observed transitions proposed in Ref. [7]. However, in the much lighter mass region, a careful analysis of time-of-flight distribution of recoils allows to some extent for identification of exit channels, especially those which involve one or two α-particles.

Because no active optical elements or scattering material are used between the target and RFD, the detector measures directly the velocity vector of each recoiling nucleus and the Doppler shift of the γ-rays emitted in flight can be corrected individually in the event-by-event mode. Due to granularity of RFD, small solid angle of the individual detection elements and the ability of precise measurement of the recoil time-of-flight, the velocity vector of the recoil is measured with high accuracy, which allows for significant improvement of the γ-ray energy resolution. The improvement in resolution achieved with RFD in fusion–evaporation reactions with a recoil velocity up to $0.05v/c$ is comparable and in many cases even better than provided by light charged particle detector arrays (Microball [31], EUCLIDES [9], DIAMANT [32]). At this recoil velocity, the energy resolution obtained with RFD is comparable also with that in γ-ray spectra with precise Doppler shift correction measured by the CLARA Ge-detector array [33] coupled to the PRISMA spectrometer for multi-nucleon transfer and deep-inelastic collisions.

Very good energy resolution in γ-ray spectra allows for evaluation of lifetimes of highly excited states in light and medium mass nuclei. The shape of the γ-ray line corrected already for Doppler shift strongly depends on the ratio of the lifetime of the state to the recoil transit time through the target. The simple method presented in the paper allows estimating lifetimes of excited states as short as few femtoseconds.

It is important to notice that in some asymmetric fusion–evaporation reactions of light projectiles at low energy with medium mass targets, the evaporation residues may be separated from the intense background of the scattered beam by their pulse height only. In consequence, the continuous beam can be applied in such cases and increasing of the beam current on a target becomes possible.

RFD is relatively small, with a dimension of the order of 1 m. It occupies a little forward space, less than 0.5% of the full solid angle. Therefore, it does not obstruct the placement of γ-ray detectors and can be coupled to any detector array or any other ancillary detectors. RFD is not sensitive to radiation damages. The mechanical construction of the individual detection elements protects plastic scintillator against direct hits by the scattered beam. In series of several days' measurements with the counting rate of 1 MHz, the reduction of the light yield of the scintillators was not observed.

RFD is considered as one option for ancillary detector to be coupled with the AGATA Demonstrator [34]. The main goal of the Demonstrator phase in the AGATA project is to prove the feasibility of the 4π γ-ray spectrometer AGATA in a realistic experiment, in particular—the tracking procedures of the γ-rays in the segmented germanium crystals. RFD should identify the fusion–evaporation reaction of the key experiment and determine the direction and velocity of the evaporation residues for the Doppler shift correction.

In experiments with radioactive beams, the high background from the decay of the beam particles likely to be encountered makes it mandatory to measure a γ-ray spectrum in coincidence with appropriate signal. The use of RFD in the fusion–evaporation measurements could provide the signal that such reaction has occurred. As radioactive beams are of low intensity, therefore, the main difficulty in handling the intense counting rates in the anticipated experiments will be less severe, while the very little radiation-sensitive mass of RFD will be a great asset.

Acknowledgements

Many people at various institutions have been involved in the design, construction and development of RFD.

The authors would like to thank them all much. Particularly, we thank W. Lahmer (then at HMI, Berlin), A. Szperłak (IFJ PAN, Krakow) and M. Rejmund (GANIL) for their help at the early stage of the project. We very much appreciate the continuous support of F.A. Beck (IReS, Strasbourg) and the help of D. Curien, N. Schulz, F. Devin and F. Kuntz (IReS, Strasbourg) during the experiments with EUROBALL IV. The authors would like to thank also A. Maj (IFJ PAN, Krakow) for the very valuable discussions on the data-acquisition system for the EUROBALL IV-RFD setup. We thank A. Czermak and B. Sowicki (IFJ PAN, Krakow) for development of the RFD fast preamplifiers. This work was supported in part by the Polish Ministry of Science and Higher Education under grant no. 1-P03B-030-30 and the French-Polish agreement IN2P3—Polish Institutions and Jumelage.

References

[1] C.N. Davids, B.B. Back, K. Bindra, D.J. Henderson, W. Kutschera, T. Lauritsen, Y. Nagame, P. Sugathan, A.V. Ramayya, W.B. Walters, Nucl. Instr. and Meth. B 70 (1992) 358.
[2] C.J. Gross, T.N. Ginter, D. Shapira, W.T. Milner, J.W. McConnell, A.N. James, J.W. Johnson, J. Mas, P.F. Mantica, R.L. Auble, J.J. Das, J.L. Blankenship, J.H. Hamilton, R.L. Robinson, Y.A. Akovali, C. Baktash, J.C. Batchelder, C.R. Bingham, M.J. Brinkman, H.K. Carter, R.A. Cunningham, T. Davinson, J.D. Fox, A. Galindo-Uribarri, R. Grzywacz, J.F. Liang, B.D. MacDonald, J. MacKenzie, S.D. Paul, A. Piechaczek, D.C. Radford, A.V. Ramayya, W. Reviol, D. Rudolph, K. Rykaczewski, K.S. Toth, W. Weintraub, C. Williams, P.J. Woods, C.-H. Yu, E.F. Zganjar, Nucl. Instr. and Meth. A 450 (2000) 12.
[3] M. Leino, J. Äysto, T. Enqvist, P. Heikkinen, A. Jokinen, M. Nurmia, A. Ostrowski, W.H. Trzaska, J. Uusitalo, K. Eskola, P. Armbruster, V. Ninov, Nucl. Instr. and Meth. B 99 (1995) 653.
[4] H. Savajols, Nucl. Instr. and Meth. B 204 (2003) 146.
[5] A.M. Stefanini, L. Corradi, G. Maron, A. Pisent, M. Trotta, A.M. Vinodkumar, S. Beghini, G. Montagnoli, F. Scarlassara, G.F. Segato, A. De Rosa, G. Inglima, D. Pierroutsakou, M. Romoli, M. Sandoli, G. Pollarolo, A. Latina, Nucl. Phys. A 701 (2002) 217c.
[6] W. Reviol, D.G. Sarantites, R.J. Charity, C.J. Chiara, J. Elson, M. Montero, O.L. Pechenaya, S.K. Ryu, L.G. Sobotka, Nucl. Instr. and Meth. A 541 (2005) 478.
[7] J. Heese, K.H. Maier, H. Grawe, J. Grebosz, H. Kluge, W. Meczynski, M. Schramm, R. Schubart, K. Spohr, J. Styczen, Phys. Lett. B 302 (1993) 390.
[8] W. Męczyński, P. Bednarczyk, R. Chapman, S. Courtin, J. Grębosz, F. Hannachi, P. Jones, J. Kownacki, M. Lach, A. Lopez-Martens, K.H. Maier, J.C. Merdinger, D. Middleton, M. Palacz, M.B. Smith, K.M. Spohr, N. Schulz, M. Ziębliński, J. Styczeń, Eur. Phys. J. A 3 (1998) 311.
[9] W. Korten, S. Lunardi, Eds., Achievements with the Euroball spectrometer 1997–2003, LNL-INFN(REP) 201/2004, ISBN88-7337-00505.
[10] J.D. Burrows, P.A. Butler, K.A. Connell, G.D. Jones, A.N. James, A.M.Y. El-Lawindy, T.P. Morrison, J. Simpson, R. Wadsworth, Nucl. Instr. and Meth. 227 (1984) 259.
[11] H. Rothard, K.O. Groeneveld, J. Kemmler, Springer Tracts Mod. Phys. 123 (1991) 97.
[12] D. Ward, G.D. Dracoulis, J.R. Leigh, R.J. Charity, D.J. Hinde, J.O. Newton, Nucl. Phys. A 406 (1983) 591.
[13] J. Galin, B. Gatty, D. Guerreau, C. Rousset, U.C. Schlottauer-Voos, X. Tarrago, Phys. Rev. C 9 (1974) 1113.
[14] K.M. Spohr, Spektroskopie der schweren neutronenarmen Kerne ^{189}Pb und ^{199}At, sowie des Kerns ^{57}Ni und Entwicklung eines Detektors für Verdampfungsrestkerne, Ph.D. Thesis, University of Bonn, 1995, and Berichte des Forschungszentrums Jülich, 1996; 3171, ISSN0944-2952.
[15] J.F. Ziegler, Particle interaction with matter, 〈http://www.srim.org〉.
[16] OPERA program, Vector-Fields Limited (GB); SIMION Program, Idaho National Engineering Laboratory, USA.
[17] J. Grębosz, Separation of nuclear fusion products by recoil filter detector—controlling the experiment and data analysis using object oriented programming, Ph.D. Thesis, IFJ PAN, Krakow, 2002.
[18] M. Ziębliński, IFJ PAN, Kraków, unpublished.
[19] P. Bednarczyk, W. Męczyński, J. Styczeń, J. Grębosz, M. Lach, A. Maj, M. Ziębliński, N. Kintz, J.C. Merdinger, N. Schulz, J.P. Vivien, A. Bracco, J. Pedroza, M.B. Smith, K.M. Spohr, Acta Phys. Pol. B 32 (2001) 747.
[20] M. Lach, J. Styczeń, W. Męczyński, P. Bednarczyk, A. Bracco, J. Grębosz, A. Maj, J.C. Merdinger, N. Schulz, M.B. Smith, K.M. Spohr, M. Ziębliński, Eur. Phys. J. A 25 (2005) 1.
[21] M. Lach, J. Styczeń, W. Męczyński, P. Bednarczyk, A. Bracco, J. Grębosz, A. Maj, J.C. Merdinger, N. Schulz, M.B. Smith, K.M. Spohr, J.P. Vivien, M. Ziębliński, Eur. Phys. J. A 16 (2003) 309.
[22] M. Lach, P. Bednarczyk, A. Bracco, J. Grębosz, M. Kadłuczka, N. Kintz, A. Maj, J.C. Merdinger, W. Męczyński, J.L. Pedroza, N. Schulz, M.B. Smith, K.M. Spohr, J. Styczeń, J.P. Vivien, M. Ziębliński, Eur. Phys. J. A 12 (2001) 381.
[23] P. Bednarczyk, J. Styczeń, A. Bracco, D. Curien, J. Grębosz, M. Lach, A. Maj, J.C. Merdinger, W. Męczyński, J. Nowacki, M.B. Smith, K. Spohr, J.P. Vivien, M. Ziębliński, Eur. Phys. J. A 20 (2004) 45.
[24] J. Dobaczewski, J.P. Vivien, K. Zuber, P. Bednarczyk, T. Byrski, D. Curien, G. De Angelis, O. Dorvaux, G. Duchene, E. Farnea, A. Gadea, B. Gall, J. Grębosz, R. Isocrate, A. Maj, W. Męczyński, J.C. Merdinger, A. Prevost, N. Redon, J. Robin, O. Stezowski, J. Styczeń, M. Ziębliński, AIP 70 (2004) 273.
[25] B. Cederwall, I.Y. Lee, S. Asztalos, M.J. Brinkman, J.A. Becker, R.M. Clark, M.A. Deleplanque, R.M. Diamond, P. Fallon, L.P. Farris, E.A. Henry, J.R. Hughes, A.O. Macchiavelli, F.S. Stephens, Nucl. Instr. and Meth. A 354 (1995) 591.
[26] C.J. Chiara, D.R. LaFosse, D.G. Sarantites, M. Devlin, F. Lerma, W. Reviol, Nucl. Instr. and Meth. A 523 (2004) 374.
[27] P. Bednarczyk et al., to be published.
[28] M. Leino, Nucl. Instr. and Meth. B 204 (2003) 129.
[29] W. Rewiol, D.G. Sarantites, C.J. Chiara, M. Montero, O.L. Pechenaya, Acta Phys. Pol. B 38 (2007) 1547.
[30] A.M. Baxter, A.P. Byrne, G.D. Dracoulis, R.V.F. Janssens, I.G. Bearden, R.G. Henry, D. Nisius, C.N. Davids, T.L. Khoo, T. Lauritsen, H. Penttilä, D.J. Henderson, M.P. Carpenter, Phys. Rev. C 48 (1993) R2140.
[31] D.G. Sarantities, P.-F. Hua, M. Devlin, L.G. Sobotka, J. Elson, J.T. Hood, D.R. LaFosse, J.E. Sarantites, M.R. Maier, Nucl. Instr. and Meth. A 381 (1996) 418.
[32] M. Aïche, M.M. Aléonard, G. Barreau, D. Boivin, F. Bourgine, D. Cabaussel, J.F. Chemin, M. Harston, J.N. Scheurer, G. La Rana, R. Moro, A. Brondi, E. Vardaci, D. Curien, F. Hannachi, Nucl. Instr. and Meth. A 508 (2003) 367.
[33] A. Gadea, D.R. Napoli, G. de Angelis, R. Menegazzo, A.M. Stefanini, L. Corradi, M. Axiotis, L. Berti, E. Fioretto, T. Kroell, A. Latina, N. Marginean, G. Maron, T. Martinez, D. Rosso, C. Rusu, N. Toniolo, S. Szilner, M. Trotta, D. Bazzacco, S. Beghini, M. Bellato, F. Brandolini, E. Farnea, R. Isocrate, S.M. Lenzi, S. Lunardi, G. Montagnoli, P. Pavan, C. Rossi Alvarez, F. Scarlassara, C. Ur, N. Blasi, A. Bracco, F. Camera, S. Leoni, B. Million, M. Pignanelli, G. Pollarolo, A. DeRosa, G. Inglima, M. La Commara, G. La Rana, D. Pierroutsakou, M. Romoli, M. Sandoli, P.G. Bizzeti, A.M. Bizzeti-Sona, G. Lo Bianco, C.M. Petrache, A. Zucchiatti, P. Cocconi, B. Quintana, Ch. Beck, D. Curien, G. Duchene, F. Haas, P. Medina, P. Papka, J. Durell, S.J. Freeman, A. Smith, B. Varley, K. Fayz, V. Pucknell, J. Simpson, W. Gelletly, P. Regan, Eur. Phys. J. A 20 (2004) 193.
[34] N. Redon, AGATA Week, Liverpool, 6–9 June 2006, 〈http://ns.ph.liv.ac.uk/AGATA/ancillary2.html〉.